# A Last Glacial Maximum forcing dataset for ocean modelling

Anne L. Morée[1], Jörg Schwinger[2]

[1]Geophysical Institute, University of Bergen and Bjerknes Centre for Climate Research, Bergen, 5007, Norway
[2]NORCE Climate, Bjerknes Centre for Climate Research, 5007 Bergen, Norway

*Correspondence to*: Anne L. Morée (anne.moree@uib.no)

**Abstract.** Model simulations of the Last Glacial Maximum (LGM, ~21 000 years before present) can aid the interpretation of proxy records, help to gain an improved mechanistic understanding of the LGM climate system and are valuable for the evaluation of model performance in a different climate state. Ocean-ice only model configurations forced by prescribed atmospheric data (referred to as "forced ocean models") drastically reduce the computational cost of paleoclimate modelling as compared to fully coupled model frameworks. While feedbacks between the atmosphere and ocean-sea-ice compartments of the Earth system are not present in such model configurations, many scientific questions can be addressed with models of this type. The data presented here are derived from fully coupled paleoclimate simulations of the Palaeoclimate Modelling Intercomparison Project (PMIP3). The data are publicly accessible at the NIRD Research Data Archive at https://doi.org/10.11582/2019.00019 (Morée and Schwinger, 2019). They consist of 2-D anomaly forcing fields suitable for use in ocean models that employ a bulk forcing approach and are optimized for use with CORE forcing fields. The data include specific humidity, downwelling longwave and shortwave radiation, precipitation, wind (v and u components), temperature and sea surface salinity (SSS). All fields are provided as climatological mean anomalies between LGM and pre-industrial times. These anomaly data can therefore be added to any pre-industrial ocean forcing data set in order to obtain forcing fields representative of LGM conditions as simulated by PMIP3 models. These forcing data provide a means to simulate the LGM in a computationally efficient way, while still taking advantage of the complexity of fully coupled model set-ups. Furthermore, the dataset can be easily updated to reflect results from upcoming and future paleo model intercomparison activities.

## 1 Introduction

The LGM (~21 kya) is of interest to the climate research community because of the relative abundance of proxy data, and because it is the most recent profoundly different climatic state of our planet. For these reasons, the LGM is extensively studied in modelling frameworks (Menviel et al., 2017; Brady et al., 2012; Otto-Bliesner et al., 2007). Model simulations of the past ocean can not only provide a method to gain a mechanistic understanding of marine proxy records, they can also inform us about model performance in a different climatic state of the Earth system (Braconnot et al., 2012). Typical state-of-the-art tools to simulate the (past) Earth system are climate or Earth system models as, for example, used in the Coupled Model Intercomparison Project phase 5 (CMIP5; Taylor et al. (2011)). Besides simulating our present climate, these CMIP5 models are also used to simulate past climate states (such as the LGM) in the Palaeoclimate Modelling Intercomparison Project 3 (PMIP3). However, the computational costs and run-time of such fully coupled model frameworks are a major obstacle for their application to palaeoclimate modelling. Palaeoclimate modelling optimally requires long (thousands to ten thousands of years) simulations in order to provide the necessary time for relevant processes to emerge (e.g. CaCO3 compensation) (Braconnot et al., 2007). Complex fully coupled models can typically not be run into full equilibrium (which requires hundreds to thousands of years of integration) due to computational costs (Eyring et al., 2016). Therefore, the PMIP3 models exhibit model drift (especially in the deep ocean, e.g. Marzocchi and Jansen (2017)). The 3$^{rd}$ phase of the PMIP project (PMIP3; Braconnot et al. (2012)) limits global mean sea-surface temperature drift to under 0.05 K per century and requires the Atlantic Meridional Overturning Circulation to be stable (Kageyama et al., 2018).

The use of PMIP output as ocean forcing is an accepted practice in ocean modelling (e.g., Muglia and Schmittner (2015)). We refer to a "forced ocean model" as a model of the ocean-sea-ice-atmosphere system in which the atmosphere is represented by prescribed 2-D forcing fields. It can be used whenever ocean-atmosphere feedbacks are of minor importance and has the advantage of reducing the computational costs – making longer or more model runs feasible. We present 2-D (surface) anomaly fields of CMIP5/PMIP3 experiments 'lgm' minus 'piControl' calculated from monthly climatological PMIP3 output. The PMIP3 output is the result of global boundary conditions and forcings (such as insolation and ice sheet cover) applied in the fully coupled PMIP3 models (Braconnot et al., 2012). Our dataset (Morée and Schwinger, 2019) is a unique compilation of existing data, processed and reformatted such that it can be readily applied in a forced ocean model framework that uses a bulk forcing approach similar to Large and Yeager (2004). Since this approach has been popularized through coordinated model intercomparison activities (Griffies et al., 2009), a majority of forced ocean models today uses this approach. The 2-D anomaly fields presented here can be added to the pre-industrial forcing of a forced ocean model in order to obtain an atmospheric forcing representative of the LGM. The data are climatological mean anomalies, and as such suitable for equilibrium LGM 'time-slice' modelling of the ocean. The description of the procedure followed to make this dataset (Sect. 3) should support any extension of the dataset with additional (PMIP-derived) variables if needed. The PMIP4 guidelines (Kageyama et al., 2017) can support users in designing a specific model set-up, for example regarding the land-sea mask, trace gas concentrations, river runoff or other conditions and forcing one would want to apply to a model. In Sect. 2, a general description of the dataset and data sources is provided alongside with an overview of the variables (Table 1).

## 2 General description of the dataset

The data presented in this article are 2-D anomaly fields of the LGM versus pre-industrial state (experiment 'lgm' minus experiment 'piControl') based on the PMIP3 (Braconnot et al., 2012). These anomaly fields can be used as atmospheric LGM forcing fields for ocean-only model set-ups when added to pre-industrial forcing fields, and are optimized for use in combination with Coordinated Ocean-ice Reference Experiments (CORE) forcing fields (Griffies et al., 2009). The use of an anomaly forcing implies the assumption that no changes in temporal or spatial variability occurred between the lgm and piControl states beyond changes in the mean. We note that by adding multi model mean anomalies to forcing fields, dynamical inconsistencies (e.g. between wind and temperature fields) could be created. A forcing data set would typically be dynamically consistent if the forcing would be the outcome of an advanced atmospheric reanalysis. However, the CORE forcing is a mixture of reanalysis and observational data products, and we assume that the addition of our anomaly fields will be a minor contribution to the dynamical inconsistencies already present in the CORE forcing fields (Large and Yeager, 2004). The basis of this data is monthly climatological PMIP3 output. Any variables presented on sub-monthly time resolution are therefore time-interpolated. Since this is a limitation of the available data, we have to assume that any sub-monthly variability (e.g. the diurnal cycle) is preserved from the preindustrial climate state to the LGM state. The anomalies are calculated as the mean of the difference between monthly climatologies of the 'lgm' and 'piControl' PMIP3 model runs. The calculation of such a model mean will dampen uncorrelated variability across the different models. However, for the sake of achieving long integration times (e.g., for paleo studies), we expect this approach is justifiable. Moreover, the calculated anomalies are generally small as compared to the forcing field itself. In cases where modelling groups provided more than one ensemble member, we included only the first member in our calculations. Even though PMIP3 simulations have limitations and a large inter-model spread, PMIP3 is the state of the art for modelling of past climates at present (Braconnot et al., 2012; Braconnot and Kageyama, 2015). Furthermore, no global proxy-based reconstructions of the variables presented here are available to provide a proxy-based LGM forcing dataset. Using mean coupled model output as forcing is thus considered the best available option for use in forced ocean models. The data is the mean anomaly of five PMIP3 models (CNRM-CM5, IPSL-CM5A-LR, GISS-E2-R, MIROC-ESM and MRI-CGCM3: Table 2), as only these models provide output for all variables.

The variables are i) specific humidity at 10 meters, ii) downwelling longwave radiation, iii) downwelling shortwave radiation, iv) precipitation, v) wind (v and u components), vi) temperature at 10 meters, and vii) sea surface salinity (SSS) (Table 1). The SSS anomaly field can be used to apply SSS restoring in LGM simulations. All variables (Sect. 3.1-7) of the monthly climatological PMIP3 output have been regridded (Table 3, #1), averaged (Table 3, #2), and differenced (Table 3, #3) to calculate the anomaly fields. Additional procedures for each variable are provided in the respective part of Sect. 3, together with a figure of each variable's yearly mean anomaly and model spread. Alongside the lgm-piControl anomaly for each variable, the model spread across all five models is made available. This inter-model disagreement is described for each variable in Sect. 3, and could for example be used to guide adjustments of the amplitude of the forcing anomaly for model tuning purposes. Additionally, proxy-base reconstructions are available for some of the variables (e.g., temperature), which can constrain potential adjustments to the forcing anomaly fields. We leave it to the individual modelling groups to make such adjustments to their forcing fields.

All operations were performed with NetCDF toolkits CDO version 1.9.3 (Schulzweida, 2019) or NCO version 4.6.9. The main functions used are documented in Table 3, and referred to in the text at the first occurrence. The atmospheric anomaly data are on a Gaussian grid, with 192×94 (lon×lat) grid-points. The SSS fields is on a regular 360×180 (lon×lat) grid. Regridding any of the files to a different model grid should be straightforward (e.g., Table 3, #1), as it was ensured that all files contain the information needed for re-gridding. The variables, grid and time resolution are chosen to be compatible with the CORE forcing fields (Large and Yeager, 2004), which have been extensively used in the ocean modelling community (e.g. Griffies et al. (2009); Schwinger et al. (2016)). We anticipate that the variables selected here should be useful in different model set-ups as well. We intend to provide a data set that is flexible with respect to the use of different land-ocean masks in different models. Therefore, we account for changes in sea-level (i.e. a larger land area in the LGM), which can affect variables in coastline areas, by applying the following masking procedure: i) masking the multi-model mean anomaly with the maximum lgm land mask across all models, then ii) extrapolating the variable over land using a distance-weighted average (Table

3, #4), and iii) finally masking the data with a present-day land mask (based on the World Ocean Atlas 2013 1° resolution land mask), but with the ocean extended in a 1.5 degrees radius over land. This choice ensures that the anomaly forcing data can be used with any pre-industrial land-sea mask. Through following this procedure, the grid points affected by land-sea mask changes are thus filled with the extrapolated model mean anomaly from the LGM coastaln ocean. In the case of NorESM-OC (Schwinger et al., 2016), the atmospheric anomaly fields were added to its CORE normal-year forcing fields (Large and Yeager, 2004) to obtain a LGM normal-year forcing, under the assumption of an unchanged spatial and temporal variability for the respective variable. Note that the addition of the anomaly fields to the user's own model forcing could lead to physically unrealistic/not-meaningful results for some variables (such as negative precipitation or radiation). This must be corrected for by capping off sub-zero values (Table 3, #5) after addition of the anomaly.

## 3 The variables

### 3.1 Specific humidity anomaly

The monthly climatology of near-surface specific humidity is provided at 2 meters height in PMIP3. The bulk forcing method of Large and Yeager (2004) requires specific humidity (and temperature) at the same height as the wind forcing (10 meters). Therefore, specific humidity was re-referenced to 10 meters height for each of the four models following the procedure detailed in Large and Yeager (2004). The re-referencing required the use of wind (u and v components), sea level pressure (CMIP variable 'psl') and skin temperature ('ts', representing sea surface temperature over the open ocean), which were taken from the respective 'piControl' and 'lgm' CMIP5/PMIP3 output for each model. The mean anomaly over the four models was time interpolated (Table 3, #6) to a 6-hour time resolution from the monthly climatological PMIP3 output. The annual mean lgm-piControl anomaly field (Fig. 1) shows a global decrease in specific humidity, as expected from decreased air temperatures (Sect. 3.6). The anomaly is most pronounced around the equator, where we see a decrease of 2-3 kg $kg^{-1}$, while the anomaly is near-zero towards both poles. The model spread of the anomaly shows a disagreement between the PMIP3 models generally in the order of 1-2 kg $kg^{-1}$, without any strong spatial pattern (Fig. 1).

### 3.2 Downwelling longwave radiation anomaly

The anomaly for surface downwelling longwave radiation is time-interpolated (Table 3, #6) to a daily time resolution. The annual mean anomaly field (Fig. 2) shows globally decreased downwelling longwave radiation in the 'lgm' experiment as compared to the 'piControl' experiment, in the order of 10-30 W $m^{-2}$ over most of the ocean due to a generally cooler atmosphere (Sect. 3.6). The largest anomalies lie close to the northern ice sheets, with up to -90 W $m^{-2}$ lower radiation in the 'lgm' experiment than in the 'piControl' experiment. Ice is likely also the main contributor to the high (60-90 W $m^{-2}$) inter-model spread in North Atlantic and Southern Oceans. The remainder of the ocean exhibits a better agreement, with inter-model spreads generally below 20 W $m^{-2}$ (Fig. 2).

### 3.3 Downwelling shortwave radiation anomaly

The surface downwelling shortwave radiation anomaly field is time-interpolated (Table 3, #6) to daily fields as done for downwelling longwave radiation. The annual mean anomaly is especially pronounced around the

Laurentide and Scandinavian ice sheets, where strong positive anomalies of over ~30 W $m^{-2}$ exist (Fig. 3). Globally, the annual mean downwelling shortwave radiation anomaly generally falls in a range of -15 to +15 W $m^{-2}$ over the ocean. The anomaly field shows negative anomalies as well positive ones in an alternating spatial pattern approximately symmetrically around the equator in the Pacific basin. The inter-model spread is largest in the North Atlantic region and along the equator (Fig. 3). Due to the large model disagreement of up to 50 W $m^{-2}$ for this variable, the inter-model spread and mean anomaly are of similar magnitude although a consistent pattern is present in the anomaly field.

### 3.4 Precipitation anomaly

The anomaly presented here is the lgm-piControl precipitation anomaly at the air-sea interface and includes both the liquid and solid phases from all types of clouds (both large-scale and convective), and excludes evaporation. The units were converted to mm $day^{-1}$ to comply with the CORE forcing format (causing a deviation from the CF-1.6 convention). The resulting annual mean anomaly generally falls in the range of -2 to 2 mm $day^{-1}$, and is most pronounced along the equator (Fig. 4). The models show a mean increase in precipitation directly south of the equator in the Pacific basin, as well as in the Pacific subtropics off the western North-American coast. The North Atlantic also receives a mean positive precipitation anomaly, offsetting part of the positive salinity anomaly there, which is potentially relevant for the simulation of deep water formation in this region (Sect. 3.7). Negative mean precipitation anomalies are most pronounced directly north of the equator and north of ~40° N in the Pacific basin as well as in the Atlantic Arctic. The inter-model spread is up to ~5 mm $day^{-1}$ around the equator, likely due to the model disagreement about the sign and location of changes in the inter-tropical convergence zone (Fig. 4). Related to precipitation fluxes, river runoff fluxes also changed between the lgm and piControl model experiments. As river routing and flux calculations are very model specific, we expect modelling groups to find a suitable solution for their setup themselves, and recommend consulting the PMIP guidelines when doing so (Kageyama et al., 2017).

### 3.5 Wind anomalies, u and v components

Both for the u and v component of the wind speed, the lgm-piControl anomaly is time-interpolated to 6-hourly fields. The annual mean meridional wind velocity (v, southerly winds) anomaly shows a pronounced increase (~3-5 m $s^{-1}$) in southerly winds around the NW edge of the Laurentide ice sheet as well as over the NW edge of the Scandinavian ice sheet (Fig. 5). Alongside that, a pronounced decrease (~ 3-5 m $s^{-1}$) in southerly winds is simulated along the eastern North American coast and the Canadian archipelago. The open ocean anomalies are generally small (at most ±1 m $s^{-1}$). The inter-model spread has no pronounced pattern but is sizable, with ~ 1-5 m $s^{-1}$ disagreement between the PMIP3 models. The mean zonal wind velocity (u, westerly winds) anomaly shows alternating negative and positive anomaly bands with an approximate ±2 m $s^{-1}$ range (Fig. 6). This pattern is stronger in the Northern Hemisphere north of ~45° N. The inter-model spread (~1-3 m $s^{-1}$) has little structure except for the ~4-5 m $s^{-1}$ disagreement in the Southern Ocean south of ~40° S, and the ~3-5 m $s^{-1}$ disagreement in the North Atlantic (Fig. 6).

### 3.6 Temperature anomaly

The near-surface atmospheric temperature at 2 m height from PMIP3 is re-referenced to 10 meters (as done for specific humidity, Sect. 3.1), and time-interpolated to calculate the 6-hourly mean anomaly for temperature. The annual mean anomaly is most pronounced in the North Atlantic, where open ocean anomalies exceed 10 K. Elsewhere, the annual mean temperature generally is around 2.5 K. There is a clear pattern in the model spread: The models show a large spread (>10 K) north of ~45° N, as well as south of ~40° S (5-10 K), likely due to the disagreement about ice cover. At lower latitudes and over the ocean the model spread is generally smaller (0-3 K) (Fig. 7).

### 3.7 Sea surface salinity anomaly

Global mean salinity is initialized in PMIP3 models with a 1 psu higher salinity to account for the concentrating effect of the decrease in sea level (Kageyama et al., 2017). Sea surface salinity however, shows a more variable annual mean lgm-piControl change due to changes in the global hydrological cycle (Fig. 8). The sea surface salinity anomaly is presented on a regular 1x1 grid for ease of use. The resulting annual mean SSS anomaly (Fig. 8) shows an increase in sea surface salinity (~1 psu) over the Southern Ocean south of ~55° S, as well as in the Arctic (>3 psu) and the Northern Indian Ocean (~1 psu). A ~2 psu anomaly is simulated in the Canadian Archipelago, the Labrador Sea and across the North Atlantic between what is now Canada and Europe (Fig. 8). Freshening is simulated close to some continents, and is especially pronounced around Scandinavia (about -3 psu). Simulated ocean circulation can be very sensitive to fresh water forcing and thus SSS, especially in the North Atlantic (e.g. Rahmstorf (1996), Spence et al. (2008)). Application of SSS restoring using the SSS anomaly field should therefore be done with caution and attention to its effects on the meridional overturning circulation. Tuning of the salinity anomaly in important deep-water formation regions of up to about ±1 psu, such as done by for example Winguth et al. (1999), may be required to obtain a satisfactory circulation field in reasonable agreement with proxy data. Such adjustments fall well within the PMIP3 model spread (Fig. 8), and show the current limitations of fully coupled PMIP3 models to simulate the LGM hydrological cycle consistent with proxy records of ocean circulation.

## 4 Data availability

The data are publicly accessible at the NIRD Research Data Archive at https://doi.org/10.11582/2019.00019 (Morée and Schwinger, 2019). The .md5 files contain an md5 checksum, which can be used to check whether changes have been made to the respective .nc files.

## 5 Summary and Conclusions

The output of the fully coupled PMIP3 simulations of CNRM-CM5, IPSL-CM5A-LR, MIROC-ESM and MRI-CGCM3 is converted to anomaly datasets intended for use in forced ocean modelling of the LGM. All anomalies are calculated as the difference between the ‘lgm’ and ‘piControl’ PMIP3 experiments. In addition, all data are formatted in a way that further conversions (of for example units or the grid) can be applied in a straightforward way. The variables are provided in NetCDF format in separate files, and distributed by the NIRD Research Data

Archive (Morée and Schwinger, 2019). A climatological LGM forcing data set can be created for any forced ocean model by addition of the presented 2-D anomaly fields to the model's pre-industrial forcing. This approach enables the scientific community to simulate the LGM ocean state in a forced model set-up. We expect that if additional forcing is needed for a specific model, the same approach as described above can be followed. This process is simplified by providing all main CDO and NCO commands used in creating the dataset (Table 3). All data represent a climatological year, i.e. one annual cycle per variable. The application of the data is thus suitable for 'time-slice' equilibrium simulations of the LGM, and optimised for use with the CORE forcing format (Large and Yeager, 2004).

The uncertainty of our anomaly forcing (approximated by the model spread of the PMIP3 models) is generally of similar magnitude as the multi-model annual mean. The attribution of the model spread to specific processes is beyond the scope of this article, but our results show that there is considerable uncertainty involved in the magnitude of the anomaly for all variables presented here. Nevertheless, all mean anomalies show a distinct spatial pattern that we expect to be indicative of the LGM-PI changes. Finally, there is no other way to reconstruct most of these variables than model simulations with state-of-the-art models such as those applied in the PMIP3 experiments. For modelling purposes, the inter-model disagreement of PMIP3 provides the user with leeway to adjust the amplitude of the forcing (guided by the size of the model spread, which is therefore provided alongside the variables in the dataset). Such adjustments can improve model-proxy data agreements, such as described for salinity in Sect. 3.7.

**Author contributions.** AM prepared, visualized and analysed the data and wrote the original draft of the manuscript. AM and JS together conceptualized the method and revised the manuscript. JS provided supervision throughout the study.

**Competing interests.** The authors declare that they have no conflict of interest.

**Acknowledgements.** We acknowledge the World Climate Research Programme's Working Group on Coupled Modelling, which is responsible for CMIP, and we thank the climate modelling groups (Table 2) for producing and making available their model output. For CMIP the U.S. Department of Energy's Program for Climate Model Diagnosis and Intercomparison provides coordinating support and led development of software infrastructure in partnership with the Global Organization for Earth System Science Portals. This is a contribution to the Bjerknes Centre for Climate Research (Bergen, Norway). Storage resources were provided by UNINETT Sigma2 - the National Infrastructure for High Performance Computing and Data Storage in Norway (project number ns2980k). Anne L. Morée is grateful for PhD funding through the Faculty for Mathematics and Natural Sciences of the University of Bergen. Jörg Schwinger acknowledges funding through the Research Council of Norway (project INES (270061)). This study is a contribution to the project "Coordinated Research in Earth Systems and Climate: Experiments, kNowledge, Dissemination and Outreach" (CRESCENDO; EU Horizon2020 Programme grant no. 641816) which is funded by the European Commission.

## References

Braconnot, P., Otto-Bliesner, B., Harrison, S., Joussaume, S., Peterchmitt, J. Y., Abe-Ouchi, A., Crucifix, M., Driesschaert, E., Fichefet, T., Hewitt, C. D., Kageyama, M., Kitoh, A., Laîné, A., Loutre, M. F., Marti, O., Merkel,

U., Ramstein, G., Valdes, P., Weber, S. L., Yu, Y., and Zhao, Y.: Results of PMIP2 coupled simulations of the Mid-Holocene and Last Glacial Maximum; Part 1: experiments and large-scale features, Clim. Past, 3, 261-277, 10.5194/cp-3-261-2007, 2007.
Braconnot, P., Harrison, S., Kageyama, M., Bartlein, P., Masson-Delmotte, V., Abe-Ouchi, A., Otto-Bliesner, B., and Zhao, Y.: Evaluation of climate models using palaeoclimatic data, Nature Climate Change, 2, 417-424, doi: 10.1038/nclimate1456, 2012.
Braconnot, P., and Kageyama, M.: Shortwave forcing and feedbacks in Last Glacial Maximum and Mid-Holocene PMIP3 simulations, Philosophical Transactions of the Royal Society A: Mathematical, Physical and Engineering Sciences, 373, 20140424, 10.1098/rsta.2014.0424, 2015.
Brady, E. C., Otto-Bliesner, B. L., Kay, J. E., and Rosenbloom, N.: Sensitivity to Glacial Forcing in the CCSM4, Journal of Climate, 26, 1901-1925, 10.1175/JCLI-D-11-00416.1, 2012.
Caubel, A., Denvil, S., Foujols, M. A., Marti, O., Dufresne, J.-L., Bopp, L., Cadule, P., Ethé, C., Idelkadi, A., Mancip, M., Masson, S., Mignot, J., Ionela, M., Balkanski, Y., Bekki, S., Bony, S., Braconnot, P., Brockman, P., Codron, F., Cozic, A., Cugnet, D., Fairhead, L., Fichefet, T., Flavoni, S., Guez, L., Guilyardi, E., Hourdin, F., Ghattas, J., Kageyama, M., Khodri, M., Labetoulle, S., Lefebvre, M.-P., Levy, C., Li, L., Lott, F., Madec, G., Marchand, M., Meurdesoif, Y., Rio, C., Schulz, M., Swingedouw, D., Szopa, S., Viovy, N., and Vuichard, N.: IPSL-CM5A-LR model output prepared for CMIP5 piControl experiment, served by ESGF,WDCC at DKRZ, doi:10.1594/WDCC/CMIP5.IPILpc, 2016.
Dufresne, J. L., Foujols, M. A., Denvil, S., Caubel, A., Marti, O., Aumont, O., Balkanski, Y., Bekki, S., Bellenger, H., Benshila, R., Bony, S., Bopp, L., Braconnot, P., Brockmann, P., Cadule, P., Cheruy, F., Codron, F., Cozic, A., Cugnet, D., de Noblet, N., Duvel, J. P., Ethé, C., Fairhead, L., Fichefet, T., Flavoni, S., Friedlingstein, P., Grandpeix, J. Y., Guez, L., Guilyardi, E., Hauglustaine, D., Hourdin, F., Idelkadi, A., Ghattas, J., Joussaume, S., Kageyama, M., Krinner, G., Labetoulle, S., Lahellec, A., Lefebvre, M. P., Lefevre, F., Levy, C., Li, Z. X., Lloyd, J., Lott, F., Madec, G., Mancip, M., Marchand, M., Masson, S., Meurdesoif, Y., Mignot, J., Musat, I., Parouty, S., Polcher, J., Rio, C., Schulz, M., Swingedouw, D., Szopa, S., Talandier, C., Terray, P., Viovy, N., and Vuichard, N.: Climate change projections using the IPSL-CM5 Earth System Model: from CMIP3 to CMIP5, Clim Dyn, 40, 2123-2165, 10.1007/s00382-012-1636-1, 2013.
Eyring, V., Bony, S., Meehl, G. A., Senior, C. A., Stevens, B., Stouffer, R. J., and Taylor, K. E.: Overview of the Coupled Model Intercomparison Project Phase 6 (CMIP6) experimental design and organization, Geosci. Model Dev., 9, 1937-1958, 10.5194/gmd-9-1937-2016, 2016.
Griffies, S. M., Biastoch, A., Böning, C., Bryan, F., Danabasoglu, G., Chassignet, E. P., England, M. H., Gerdes, R., Haak, H., Hallberg, R. W., Hazeleger, W., Jungclaus, J., Large, W. G., Madec, G., Pirani, A., Samuels, B. L., Scheinert, M., Gupta, A. S., Severijns, C. A., Simmons, H. L., Treguier, A. M., Winton, M., Yeager, S., and Yin, J.: Coordinated Ocean-ice Reference Experiments (COREs), Ocean Modelling, 26, 1-46, https://doi.org/10.1016/j.ocemod.2008.08.007, 2009.
JAMSTEC, AORI, and NIES: MIROC-ESM model output prepared for CMIP5 piControl, served by ESGF, doi:10.1594/WDCC/CMIP5.MIMEpc 2015a.
JAMSTEC, AORI, and NIES: MIROC-ESM model output prepared for CMIP5 lgm, served by ESGF, doi:10.1594/WDCC/CMIP5.MIMElg, 2015b.
Kageyama, M., Denvil, S., Foujols, M. A., Caubel, A., Marti, O., Dufresne, J.-L., Bopp, L., Cadule, P., Ethé, C., Idelkadi, A., Mancip, M., Masson, S., Mignot, J., Ionela, M., Balkanski, Y., Bekki, S., Bony, S., Braconnot, P., Brockman, P., Codron, F., Cozic, A., Cugnet, D., Fairhead, L., Fichefet, T., Flavoni, S., Guez, L., Guilyardi, E., Hourdin, F., Ghattas, J., Khodri, M., Labetoulle, S., Lefebvre, M.-P., Levy, C., Li, L., Lott, F., Madec, G., Marchand, M., Meurdesoif, Y., Rio, C., Schulz, M., Swingedouw, D., Szopa, S., Viovy, N., and Vuichard, N.: IPSL-CM5A-LR model output prepared for CMIP5 lgm experiment, served by ESGF,WDCC at DKRZ doi:10.1594/WDCC/CMIP5.IPILlg, 2016.
Kageyama, M., Albani, S., Braconnot, P., Harrison, S. P., Hopcroft, P. O., Ivanovic, R. F., Lambert, F., Marti, O., Peltier, W. R., Peterschmitt, J. Y., Roche, D. M., Tarasov, L., Zhang, X., Brady, E. C., Haywood, A. M., LeGrande, A. N., Lunt, D. J., Mahowald, N. M., Mikolajewicz, U., Nisancioglu, K. H., Otto-Bliesner, B. L., Renssen, H., Tomas, R. A., Zhang, Q., Abe-Ouchi, A., Bartlein, P. J., Cao, J., Li, Q., Lohmann, G., Ohgaito, R., Shi, X., Volodin, E., Yoshida, K., Zhang, X., and Zheng, W.: The PMIP4 contribution to CMIP6 – Part 4: Scientific objectives and experimental design of the PMIP4-CMIP6 Last Glacial Maximum experiments and PMIP4 sensitivity experiments, Geosci. Model Dev., 10, 4035-4055, 10.5194/gmd-10-4035-2017, 2017.
Kageyama, M., Braconnot, P., Harrison, S. P., Haywood, A. M., Jungclaus, J. H., Otto-Bliesner, B. L., Peterschmitt, J. Y., Abe-Ouchi, A., Albani, S., Bartlein, P. J., Brierley, C., Crucifix, M., Dolan, A., Fernandez-Donado, L., Fischer, H., Hopcroft, P. O., Ivanovic, R. F., Lambert, F., Lunt, D. J., Mahowald, N. M., Peltier, W. R., Phipps, S. J., Roche, D. M., Schmidt, G. A., Tarasov, L., Valdes, P. J., Zhang, Q., and Zhou, T.: The PMIP4 contribution to CMIP6 – Part 1: Overview and over-arching analysis plan, Geosci. Model Dev., 11, 1033-1057, 10.5194/gmd-11-1033-2018, 2018.

Large, W. G., and Yeager, S. G.: Diurnal to decadal global forcing for ocean and sea-ice models: the data sets and flux climatologies, Tech. Note NCAR/TN-460+STR. National Center of Atmospheric Research, Boulder, Colorado, USA, http://opensky.ucar.edu/islandora/object/technotes:434, 2004.

Marzocchi, A., and Jansen, M. F.: Connecting Antarctic sea ice to deep-ocean circulation in modern and glacial climate simulations, Geophysical Research Letters, 44, 6286-6295, 10.1002/2017GL073936, 2017.

Menviel, L., Yu, J., Joos, F., Mouchet, A., Meissner, K. J., and England, M. H.: Poorly ventilated deep ocean at the Last Glacial Maximum inferred from carbon isotopes: A data-model comparison study, Paleoceanography, 32, 2-17, 10.1002/2016pa003024, 2017.

Morée, A., Schwinger, J.: PMIP3-based Last Glacial Maximum (LGM) pre-industrial (PI) anomaly fields for addition to PI ocean model forcing, version 2, Norstore, https://doi.org/10.11582/2019.00019, 2019.

Muglia, J., and Schmittner, A.: Glacial Atlantic overturning increased by wind stress in climate models, Geophysical Research Letters, 42, 9862-9868, doi:10.1002/2015gl064583, 2015.

NASA-GISS: GISS-E2-R model output prepared for CMIP5 pre-industrial control, served by ESGF WDCC at DKRZ, doi:10.1594/WDCC/CMIP5.GIGRpc, 2014a.

NASA-GISS: GISS-E2-R model output prepared for CMIP5 last glacial maximum, served by ESGF WDCC at DKRZ, doi:10.1594/WDCC/CMIP5.GIGRlg, 2014b.

Otto-Bliesner, B. L., Hewitt, C. D., Marchitto, T. M., Brady, E., Abe-Ouchi, A., Crucifix, M., Murakami, S., and Weber, S. L.: Last Glacial Maximum ocean thermohaline circulation: PMIP2 model intercomparisons and data constraints, Geophysical Research Letters, 34, 10.1029/2007GL029475, 2007.

Rahmstorf, S.: On the freshwater forcing and transport of the Atlantic thermohaline circulation, Clim Dyn, 12, 799-811, 10.1007/s003820050144, 1996.

Schmidt, G. A., Kelley, M., Nazarenko, L., Ruedy, R., Russell, G. L., Aleinov, I., Bauer, M., Bauer, S. E., Bhat, M. K., Bleck, R., Canuto, V., Chen, Y.-H., Cheng, Y., Clune, T. L., Del Genio, A., de Fainchtein, R., Faluvegi, G., Hansen, J. E., Healy, R. J., Kiang, N. Y., Koch, D., Lacis, A. A., LeGrande, A. N., Lerner, J., Lo, K. K., Matthews, E. E., Menon, S., Miller, R. L., Oinas, V., Oloso, A. O., Perlwitz, J. P., Puma, M. J., Putman, W. M., Rind, D., Romanou, A., Sato, M., Shindell, D. T., Sun, S., Syed, R. A., Tausnev, N., Tsigaridis, K., Unger, N., Voulgarakis, A., Yao, M.-S., and Zhang, J.: Configuration and assessment of the GISS ModelE2 contributions to the CMIP5 archive, Journal of Advances in Modeling Earth Systems, 6, 141-184, 10.1002/2013MS000265, 2014.

Schulzweida, U.: CDO User Guide (Version 1.9.6), Max Planck Institute for Meteorology, Bundesstraße 53, 20146 Hamburg, Germany, http://doi.org/10.5281/zenodo.2558193, 215 pp., 2019.

Schwinger, J., Goris, N., Tjiputra, J. F., Kriest, I., Bentsen, M., Bethke, I., Ilicak, M., Assmann, K. M., and Heinze, C.: Evaluation of NorESM-OC (versions 1 and 1.2), the ocean carbon-cycle stand-alone configuration of the Norwegian Earth System Model (NorESM1), Geosci. Model Dev., 9, 2589-2622, 10.5194/gmd-9-2589-2016, 2016.

Sénési, S., Richon, J., Franchistéguy, L., Tyteca, S., Moine, M.-P., Voldoire, A., Sanchez-Gomez, E., Salas y Mélia, D., Decharme, B., Cassou, C., Valcke, S., Beau, I., Alias, A., Chevallier, M., Déqué, M., Deshayes, J., Douville, H., Madec, G., Maisonnave, E., Planton, S., Saint-Martin, D., Szopa, S., Alkama, R., Belamari, S., Braun, A., Coquart, L., and Chauvin, F.: CNRM-CM5 model output prepared for CMIP5 piControl, served by ESGF,WDCC at DKRZ, doi:10.1594/WDCC/CMIP5.CEC5pc, 2014a.

Sénési, S., Richon, J., Franchistéguy, L., Tyteca, S., Moine, M.-P., Voldoire, A., Sanchez-Gomez, E., Salas y Mélia, D., Decharme, B., Cassou, C., Valcke, S., Beau, I., Alias, A., Chevallier, M., Déqué, M., Deshayes, J., Douville, H., Madec, G., Maisonnave, E., Planton, S., Saint-Martin, D., Szopa, S., Alkama, R., Belamari, S., Braun, A., Coquart, L., and Chauvin, F.: CNRM-CM5 model output prepared for CMIP5 lgm, served by ESGF,WDCC at DKRZ, doi:10.1594/WDCC/CMIP5.CEC5lg, 2014b.

Spence, J. P., Eby, M., and Weaver, A. J.: The Sensitivity of the Atlantic Meridional Overturning Circulation to Freshwater Forcing at Eddy-Permitting Resolutions, Journal of Climate, 21, 2697-2710, 10.1175/2007JCLI2103.1, 2008.

Sueyoshi, T., Ohgaito, R., Yamamoto, A., Chikamoto, M. O., Hajima, T., Okajima, H., Yoshimori, M., Abe, M., O'Ishi, R., Saito, F., Watanabe, S., Kawamiya, M., and Abe-Ouchi, A.: Set-up of the PMIP3 paleoclimate experiments conducted using an Earth system model, MIROC-ESM, Geosci. Model Dev., 6, 819-836, 10.5194/gmd-6-819-2013, 2013.

Taylor, K. E., Stouffer, R. J., and Meehl, G. A.: An Overview of CMIP5 and the Experiment Design, Bulletin of the American Meteorological Society, 93, 485-498, 10.1175/BAMS-D-11-00094.1, 2011.

Voldoire, A., Sanchez-Gomez, E., Salas y Mélia, D., Decharme, B., Cassou, C., Sénési, S., Valcke, S., Beau, I., Alias, A., Chevallier, M., Déqué, M., Deshayes, J., Douville, H., Fernandez, E., Madec, G., Maisonnave, E., Moine, M. P., Planton, S., Saint-Martin, D., Szopa, S., Tyteca, S., Alkama, R., Belamari, S., Braun, A., Coquart, L., and Chauvin, F.: The CNRM-CM5.1 global climate model: description and basic evaluation, Clim Dyn, 40, 2091-2121, 10.1007/s00382-011-1259-y, 2013.

Winguth, A. M. E., Archer, D., Duplessy, J. C., Maier-Reimer, E., and Mikolajewicz, U.: Sensitivity of paleonutrient tracer distributions and deep-sea circulation to glacial boundary conditions, Paleoceanography, 14, 304-323, 10.1029/1999PA900002, 1999.

Yukimoto, S., Adachi, Y., Hosaka, M., Sakami, T., Yoshimura, H., Hirabara, M., Tanaka, T. Y., Shindo, E., Tsujino, H., Deushi, M., Mizuta, R., Yabu, S., Obata, A., Nakano, H., Koshiro, T., Ose, T., and Kitoh, A.: A New Global Climate Model of the Meteorological Research Institute: MRI-CGCM3;Model Description and Basic Performance, Journal of the Meteorological Society of Japan. Ser. II, 90A, 23-64, 10.2151/jmsj.2012-A02, 2012.

Yukimoto, S., Adachi, Y., Hosaka, M., Sakami, T., Yoshimura, H., Hirabara, M., Tanaka, T., Shindo, E., Tsujino, H., Deushi, M., Mizuta, R., Yabu, S., Obata, A., Nakano, H., Koshiro, T., Ose, T., and Kitoh, A.: MRI-CGCM3 model output prepared for CMIP5 piControl, served by ESGF,WDCC at DKRZ, doi:10.1594/WDCC/CMIP5.MRMCpc, 2015a.

Yukimoto, S., Adachi, Y., Hosaka, M., Sakami, T., Yoshimura, H., Hirabara, M., Tanaka, T., Shindo, E., Tsujino, H., Deushi, M., Mizuta, R., Yabu, S., Obata, A., Nakano, H., Koshiro, T., Ose, T., and Kitoh, A.: MRI-CGCM3 model output prepared for CMIP5 lgm, served by ESGF,WDCC at DKRZ, doi:10.1594/WDCC/CMIP5.MRMClg, 2015b.

| Variable description | Units | Resolution (lon×lat), time | Notes | Variable name | PMIP3 variable name(s) |
|---|---|---|---|---|---|
| Specific humidity | kg $kg^{-1}$ | 192×94, 1460 | Re-referenced to 10 m | huss_10m | huss |
| Downwelling longwave radiation | W $m^{-2}$ | 192×94, 365 | | rlds | rlds |
| Downwelling shortwave radiation | W $m^{-2}$ | 192×94, 365 | | rsds | rsds |
| Precipitation | mm $day^{-1}$ | 192×94, 12 | | pr | pr |
| Wind (u and v components) | m $s^{-1}$ | 192×94, 1460 | | uas and vas | uas and vas |
| Temperature | K | 192×94, 1460 | Re-referenced to 10 m | tas_10m | tas |
| Sea surface salinity | psu | 360×180, 12 | | sos | so |

**Table 1: Summary of the data showing variable description, units, format (lon×lat, time), Notes, NetCDF variable name(s) and the original PMIP3 variable name(s). Formats follow CORE conventions (Large and Yeager, 2004). The wind component variables are provided in separate files (Morée and Schwinger, 2019). In each NetCDF file (i.e., for each variable) the model spread is provided alongside the anomaly field named 'variablename_spread'.**

| Model name | Modelling group | Reference | Source data reference |
|---|---|---|---|
| CNRM-CM5 | CNRM-CERFACS (France) | Voldoire et al. (2013) | piControl: Sénési et al. (2014a)<br>lgm: Sénési et al. (2014b) |
| IPSL-CM5A-LR | IPSL (Institut Pierre Simon Laplace, France) | Dufresne et al. (2013) | piControl: Caubel et al. (2016)<br>lgm: Kageyama et al. (2016) |
| MIROC-ESM | MIROC (JAMSTEC and NIES, Japan) | Sueyoshi et al. (2013) | piControl: JAMSTEC et al. (2015a)<br>lgm: JAMSTEC et al. (2015b) |
| MRI-CGCM3 | MRI (Meteorological Research Institute, Japan) | Yukimoto et al. (2012) | piControl: Yukimoto et al. (2015a)<br>lgm: Yukimoto et al. (2015b) |
| GISS-E2-R | NASA/GISS (Goddard Institute for Space Studies, USA) | Schmidt et al. (2014) | piControl: NASA-GISS (2014a)<br>lgm: NASA-GISS (2014b) |

**Table 2: PMIP3 models used in this study**

| # | CDO or NCO command |
|---|---|
| 1 | cdo remapbil,t62grid |
| 2 | cdo ensmean |
| 3 | cdo sub |
| 4 | cdo setmisstodis |
| 5 | ncap2 |
| 6 | cdo inttime |

**Table 3: Package commands applied in this study. Detailed information on these commands can be found in the respective NCO and CDO documentation online. All operations were performed with either CDO version 1.9.3 (Schulzweida, 2019) or NCO version 4.6.9. The complete list of commands is available in the NetCDF files as global attribute 'history'.**

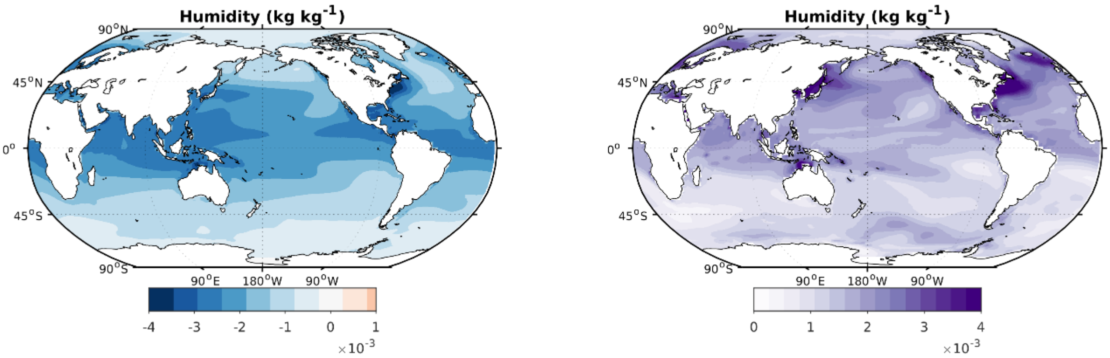


**Figure 1: Annual mean 10-meter height specific humidity lgm-piControl anomaly (left) and model spread (right) in kg kg$^{-1}$.**

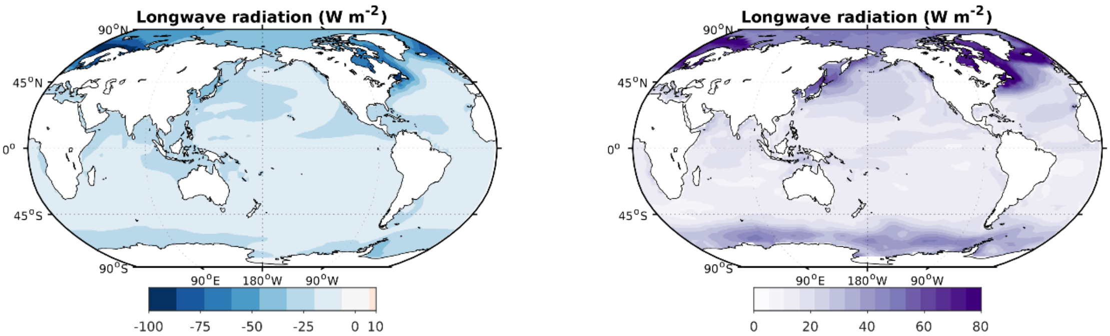


**Figure 2: Annual mean downwelling longwave radiation lgm-piControl anomaly (left) and model spread (right) in W m$^{-2}$.**

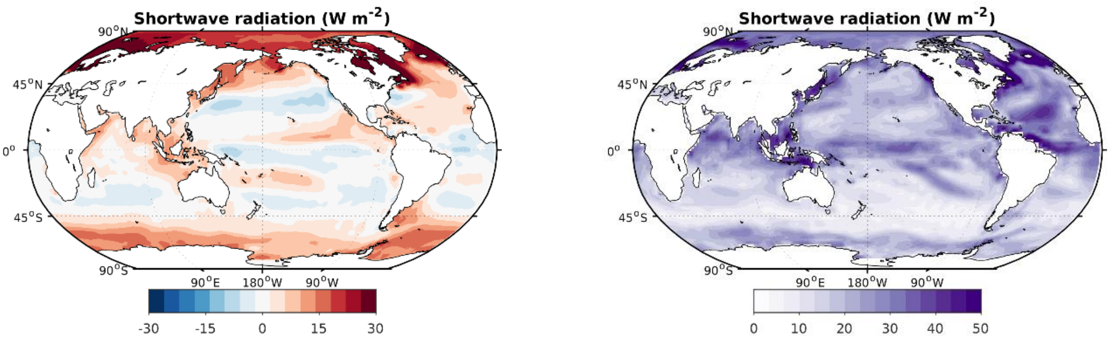


**Figure 3: Annual mean downwelling shortwave radiation lgm-piControl anomaly (left) and model spread (right) in W m$^{-2}$.**

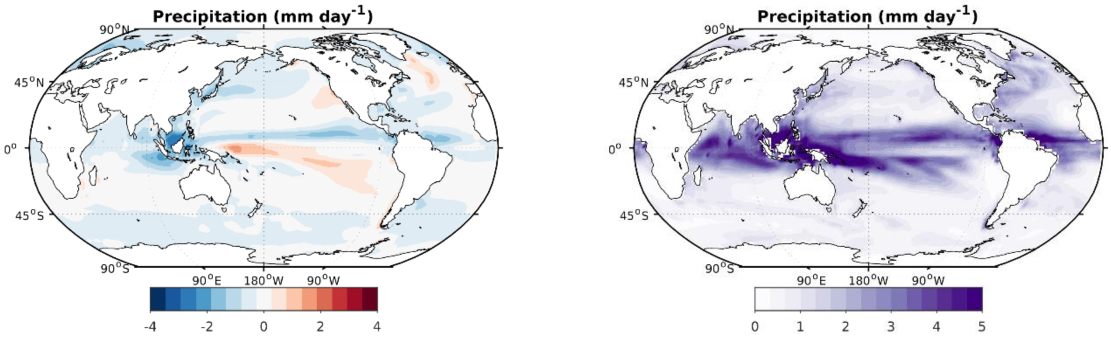


**Figure 4: Annual mean precipitation lgm-piControl anomaly (left) and model spread (right) in mm day$^{-1}$.**

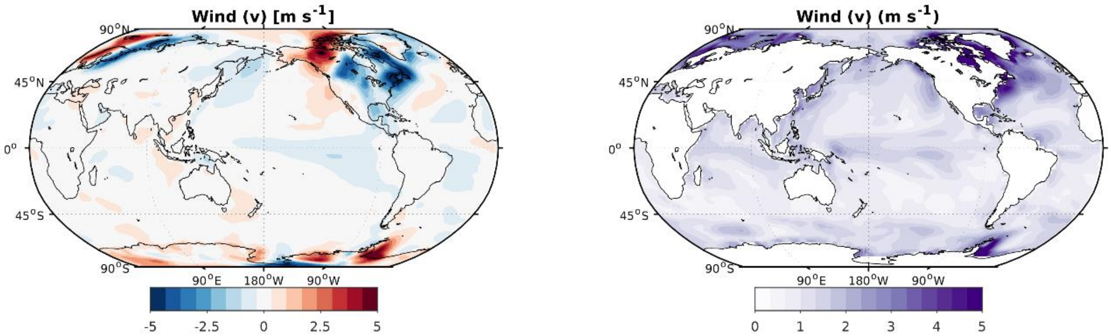


**Figure 5: Annual mean meridional wind velocity lgm-piControl anomaly (left) and model spread (right) in m s$^{-1}$.**

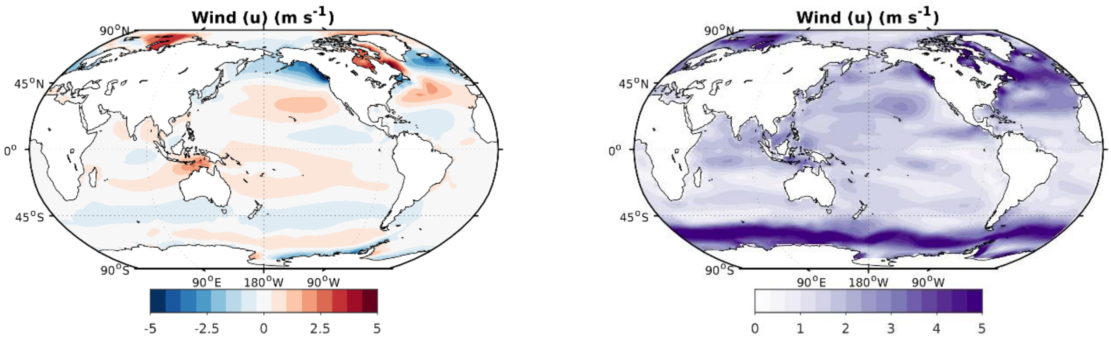


**Figure 6: Annual mean zonal wind velocity lgm-piControl anomaly (left) and model spread (right) in m s$^{-1}$.**

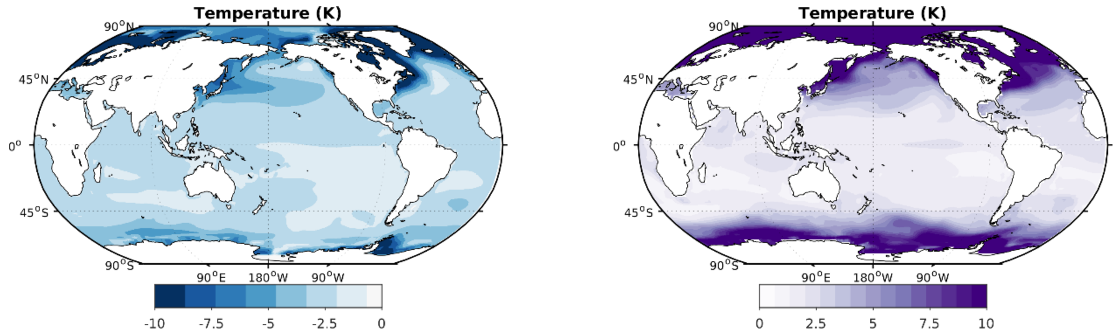


**Figure 7: Annual mean 10-meter height temperature lgm-piControl anomaly (left) and model spread (right) in K.**

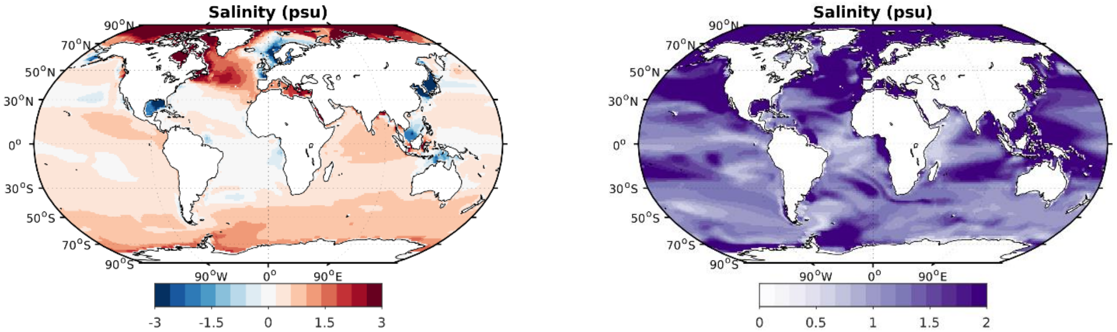


**Figure 8: Annual mean sea surface salinity lgm-piControl anomaly (left) and model spread (right) in psu.**